FMOS: the fiber multiple-object spectrograph IV: current status of OHS-based spectrograph

Fumihide Iwamuro[a], Toshinori Maihara[a], Kouji Ohta[a], Shigeru Eto, Michinari Sakai[a], Masayuki Akiyama[b], Masahiko Kimura[b], Naoyuki Tamura[b], Junichi Noumaru[b], Hiroshi Karoji[b], Gavin B. Dolton[c], Ian J. Lewis[c], Ian A. J. Tosh[d], Graham J. Murray[e], Nigel A. Dipper[e], David J. Robertoson[e], Peter R. Gillingham[f], Scott Smedley[f], Greg A. Smith[f], G. Frost[f]

[a]Department of Astronomy, Kyoto University, Kitashirakawa, Kyoto, Japan;
[b]Subaru Telescope, National Astronomical Observatory of Japan, Hilo, HI, 96720;
[c]Department of Physics, University of Oxford, Keble Road, Oxford, OX1 3RH, UK;
[d]CCLRC Rutherford Appleton Laboratory, Chilton, Didcot, Oxfordshire, OX11 0QX, UK;
[e]Department of Physics, University of Durham, South Road, Durham, DH1 3LE, UK;
[f]Anglo-Australian Observatory, P.O. Box 296, Epping, NSW 2121, Australia

ABSTRACT

The Fiber Multiple-Object Spectrograph for Subaru Telescope (FMOS) is quite large instrument composed of the prime focus unit, the fiber bundle unit, and the two infrared spectrographs. Among these units, a part of the prime focus unit and one of the spectrograph were transported from Kyoto University to the Subaru observatory in the middle of 2005. We present the optical and the mechanical components of the spectrograph, which was reassembled on the new floor of the Subaru dome. We also show the preliminary results of the optical alignment and the cooling test of the instrument at the summit of Mauna Kea.

Keywords: Infrared, Spectrograph, Fiber

1. INTRODUCTION

FMOS: the Fiber Multiple-Object Spectrograph[1–3] is the next common-use instrument of the Subaru Telescope, which has the capability of 400 targets multiplicity in the near-infrared $0.9-1.8\mu$m wavelength range with a field coverage of $30'$ diameter. FMOS consists of three units: 1) the prime focus unit including the corrector lenses, the Echidna[4–6] fiber positioner, and the instrument-bay to adjust the instrument focus and shift the axis of the corrector lens system, 2) the fiber bundle unit equipping two fiber slits (200 fibers in each) on one end and a fiber connector box[7] with the back-illumination mechanism on the other end on the bundle, 3) the two infrared spectrographs (IRS1 and IRS2) to obtain 2×200 spectra simultaneously. In these parts, the fiber positioner and the corrector lens system in the prime focus unit are developed by AAO,[8] the fiber bundle unit is by University of Durham, one of the spectrographs (IRS2)[9,10] is by University of Oxford and Rutherford Appleton Laboratory, and the other spectrograph (IRS1) and the instrument-bay in the prime focus unit are developed by Kyoto University. In this paper, we report the details of IRS1 near completion. The optical and mechanical components of the spectrograph are described in section 2 and 3, and the results of the preliminary tests are presented in section 4.

2. OPTICAL COMPONENTS

Fig. 1 shows the optical layout of IRS1. All the optical components and parameters of IRS1 are identical with those of IRS2. These spectrographs are designed to have a capability of OH-airglow suppression (OHS)[11] by focusing the primary spectra onto the mask mirror. The secondary spectra are obtained by the 2048×2048 infrared array detector HAWAII2[12] installed in the cryostat camera system. The length of the incident fiber slit

Further author information: (Send correspondence to F.I.)
F.I.: E-mail: iwamuro@kusastro.kyoto-u.ac.jp, Telephone: 81 75 753 3891

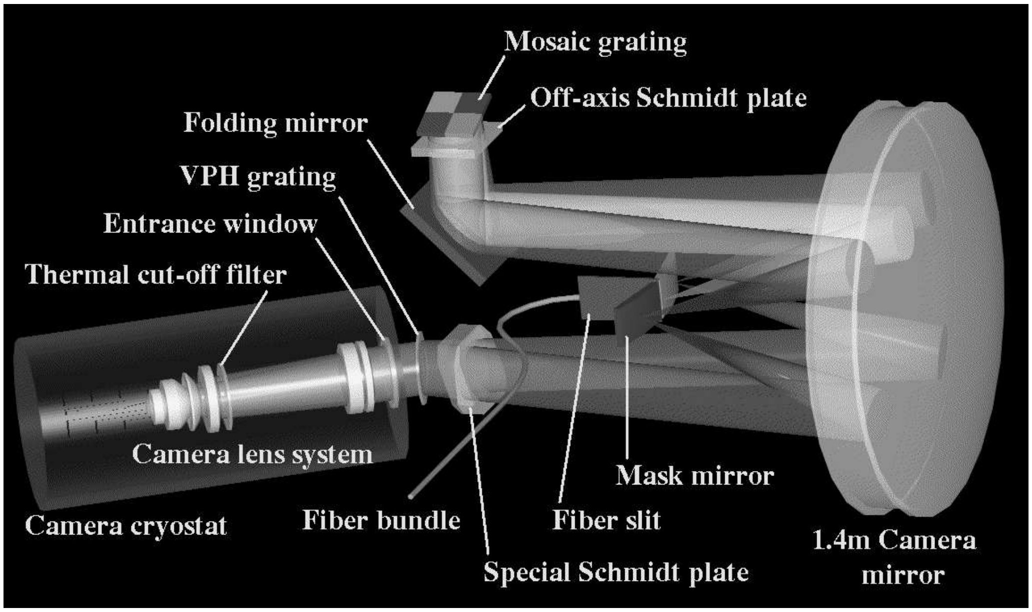

Figure 1. Optical design of IRS1. Optical system from the incident fiber slit to the mask mirror (upper half of the drawing) is the double-path Schmidt system. The reflective mosaic grating and the VPH grating are located at the primary and the secondary pupil, while the primary and the secondary spectra are focused onto the mask mirror and the detector, respectively.

is 12cm, which is reduced to $\sim$ 4cm on the detector. Although the typical spectral resolution of the primary spectra is 2200, we can choose the spectral resolution of the secondary spectra 500 (low-dispersion mode) or 2200 (high-dispersion mode) with/without the VPH grating into the optical path at secondary pupil position to reduce the dispersion given by the first grating. The spectra with the full wavelength range ($0.9-1.8\mu$m) are obtained by single exposure in the low-dispersion mode, while we need four exposures at different camera positions to cover the same wavelength range in the high-dispersion mode. All of the optical component must be cooled to reduce the thermal background because of no cold slit in the optical path. Hereafter, we make a brief comment on individual optical elements.

The fiber slit being developed by University of Durham contains 200 fibers with a spacing of 600μm and 250μm core diameter. In addition to this, we prepared another fiber bundle for the test of IRS1. The fiber slit attached to one end of this test bundle consists of 247 fibers with a spacing of 480μm and 200μm core diameter, while on the other end of fibers are packed into a square-shaped aperture. The fibers in this fiber slit are arranged in a fan shape along the curvature of the focal sphere of the Schmidt optical system of IRS1, which is achieved by an alignment jig with 247 grooves (Fig. 2) cut by a numerical control thin disk cutter. The focal ratio of the output beam from the fiber is F/5.

The spherical camera mirror is a honeycomb light-weighted mirror with a diameter of 1.4m and a weight of 137kg manufactured by Hextek Corp.* The radius of the curvature is 1940mm, or the distance of 951mm between the fiber slit and this mirror, giving the single beam diameter of $\sim$200mm. The reflective surface is silver with sapphire overcoating.

The off-axis Schmidt plate with dimensions of 280mm$\times$236mm ($\times$33mm in thickness) is manufactured by NAGASE INTEGREX Co.,Ltd. † using high-accuracy grinding processing (without polishing). The accuracy of the total shape is 0.3μm and the local roughness is 80nm rms. The material is fused silica with antireflection coatings on both sides.

*http://www.hextek.com

†http://www.nagase-i.co.jp/html_doc/new_top/html/top/tope.htm

Figure 2. Alignment jig for the test fiber slit. Total 247 fibers are fixed in the groove individually.

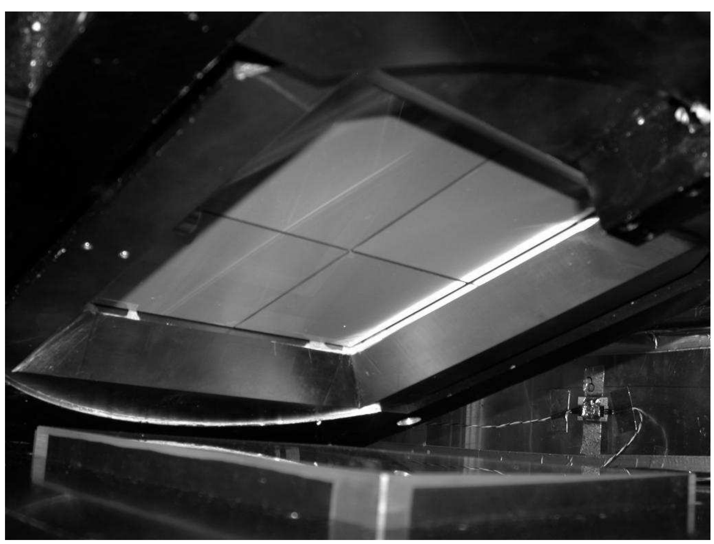

Figure 3. Mosaic reflective grating at the primary pupil position.

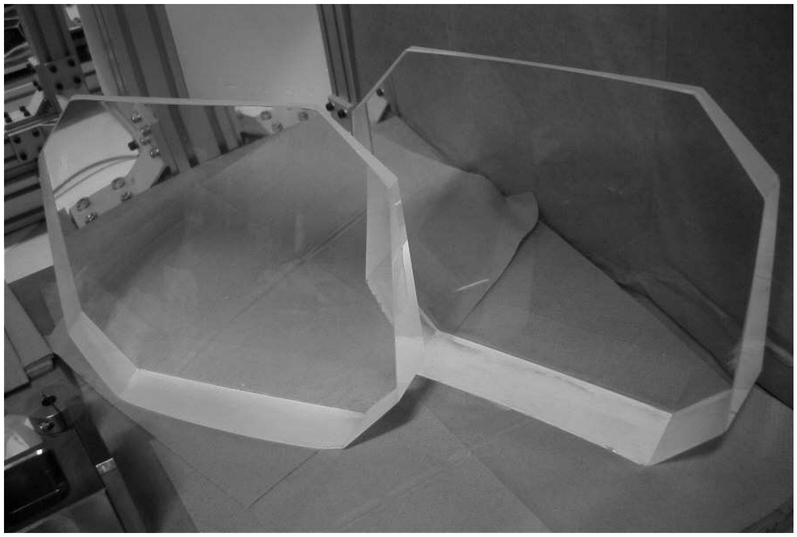

Figure 4. Two elements of the special Schmidt plate. The left side element has convex surface while the right side one has concave surface.

The grating at the primary pupil position is composed of 2×2 mosaic of usual reflective gratings with a groove density of 500 g/mm blazed at 1.4μm for the incident angle of 20°, because the diffraction limited performance is not required and the cost reduced considerably (Fig. 3). The total dimensions of this grating is 230mm × 210mm. We adopt CLEARCERAM-Z[‡] as a substrate material. The groove surfaces is coated by aluminum.

The mask mirror consists of the two spherical-convex mirrors with a curvature radius of 993mm. Each mirror has dimensions of 280mm×140mm, arranged at both sides of the entrance fiber slit. The gap between these two mirrors corresponds to the atmospheric absorption band at ∼1.4μm in the primary spectra focused onto these mirrors. The methods of masking strong OH-airglow lines are different between IRS1 and IRS2. The airglow mask of IRS2 is printed directory on the surface of the mirror by changing the coating material along the positions of the strong OH lines, while the mask of IRS1 is made of a thin (0.2mm in thickness) stainless-steel plate processed by photochemical etching. The reflective surface of the IRS1 mask mirror is aluminum with SiO_2 overcoating.

The special Schmidt plate has two aspherical concave/convex surfaces with dimensions of 315mm×251mm (× ∼90mm in thickness), which are achieved by a combination of two elements having concave-flat and flat-convex shape (Fig. 4). Both aspherical surfaces are processed by "ELID" (ELectrolytic In-process Dressing) grinding method at RIKEN[§] in Japan. The accuracy of the total shape is 3μm and the local roughness is 100nm rms. The material is fused silica with an antireflection coating on the flat side of each element (the coating on the aspherical side is TBD).

The VPH grating with a diameter of 262mmϕ and 10mm in thickness is used at the secondary pupil to reduce the dispersion power in the low-dispersion mode. The groove density is 372 g/mm. The material of the substrate is BK7 with antireflection coatings on both side.

The camera lens system in the cryostat consists of 5 spherical lenses, an entrance window, and the thermal cut-off filter with the cut-off wavelength of 1.9μm. The material of all the camera elements is fused silica with the maximum diameter of 250mm. The first order of the axial chromatic aberration of this system is corrected by tilting the detector along the dispersion axis. The focus position and this tilt angle are adjusted to the best position of the selected observation mode.

[‡]http://www.ohara-inc.co.jp/en/product/special/clearceram.html
[§]http://www.riken.go.jp

Figure 5. Refrigerator of IRS1.

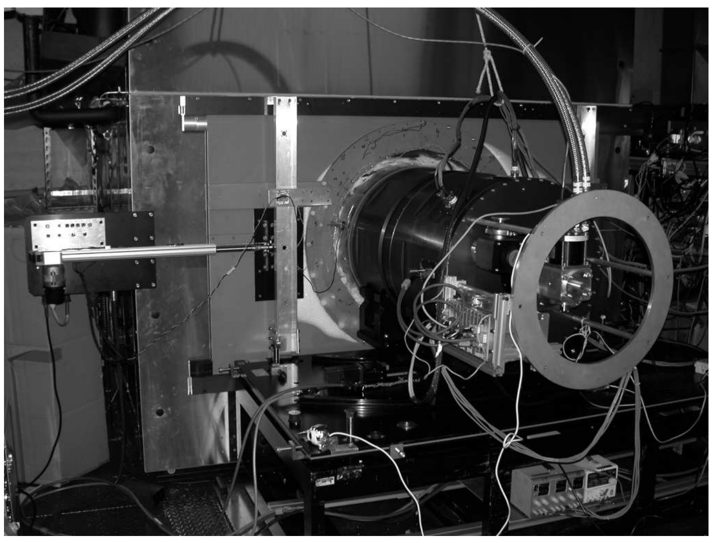

Figure 6. Camera on the circular-arc guiding stage.

3. MECHANICAL COMPONENTS

Although the basic concepts of the mechanical structure is the same in the two spectrographs, the real mechanical components are completely different. In this section, we give brief descriptions of individual mechanical components of IRS1.

The largest component in IRS1 is the refrigerator to keep the temperature of the inside optics below −50°C. The height, width, and breadth of this refrigerator are 2.4m, 2.3m, and 2.9m respectively (Fig. 5). The −60°C refrigerant gas flows through the tubes embedded in the adiabatic wall with a thickness of ∼20cm. There are a few warm wall parts around the camera cryostat and the door, which are covered with the radiation shield screen to reduce the infrared stray light inside of the refrigerator. The inside temperatures measured at 19 different positions and also the inside humidity at one position are referred to control the compressor of the refrigerator from the control PC. The dry air with a dew-point temperature of −60°C is constantly supplied through the

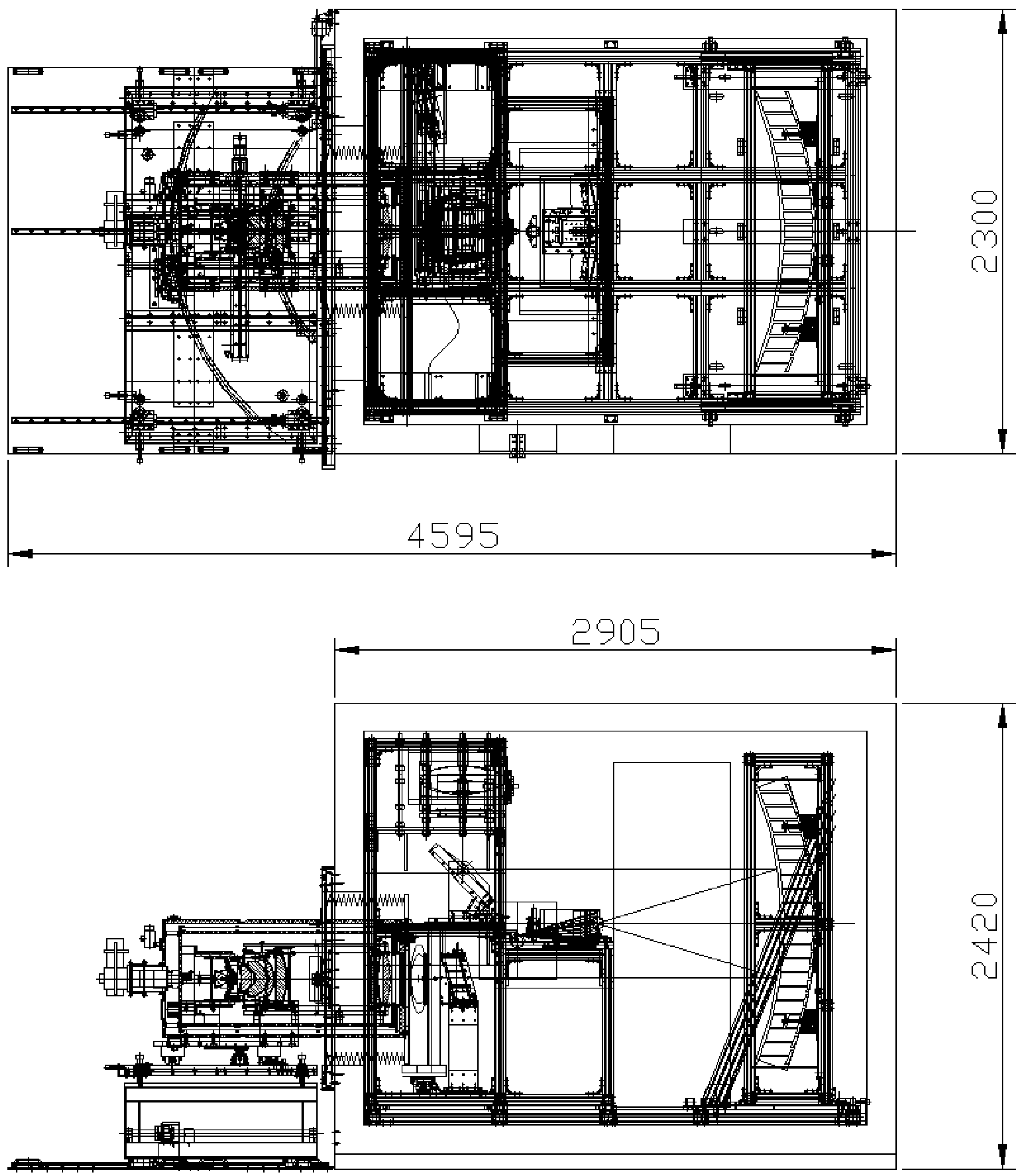

Figure 7. Optical bench design of IRS1.

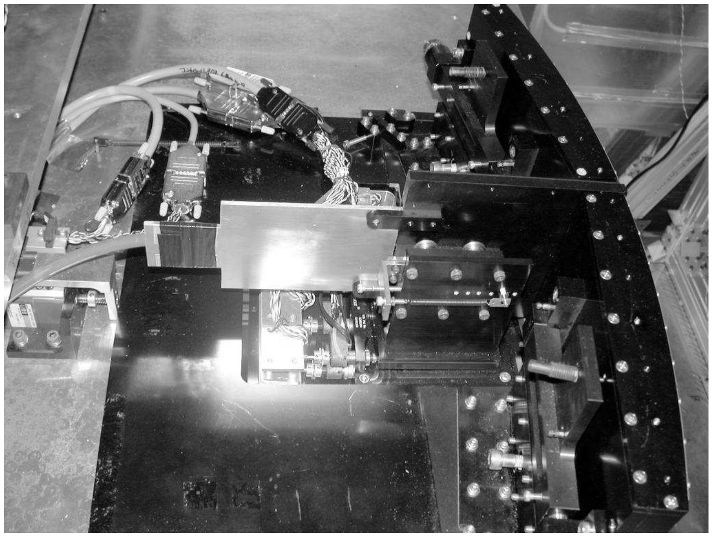

Figure 8. Mask mirror stage and 6-axis adjustable slit stage with Picomotor^{TM} actuators.

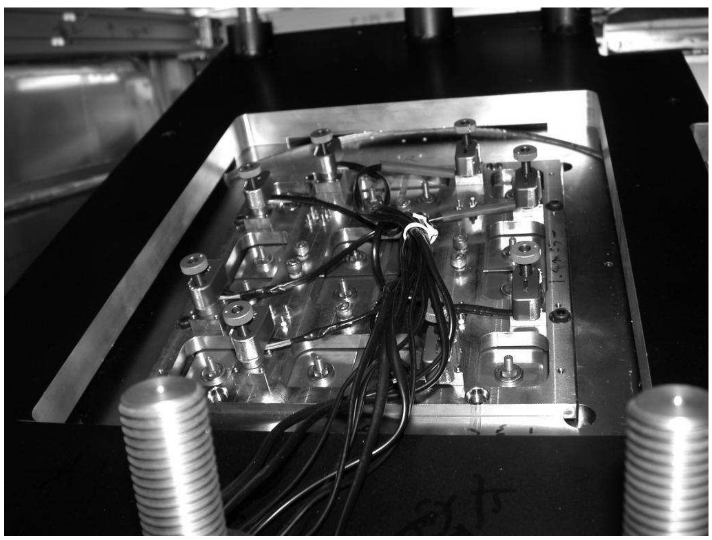

Figure 9. Mosaic grating holder with 8 Picomotor^{TM} actuators.

membrane air dryer to avoid dew condensation ice on the optics. We have to cool down the inside temperature slowly to keep the contraction speed of the inside air smaller than the flow rate of the dry air.

The camera cryostat with dimensions of 610mm$\phi\times$1280mm is attached to the refrigerator through a large hole in one of the wall panelings (Fig. 6 and Fig. 7). Since the position of this cryostat must be rotated around the virtual axis located at the secondary pupil, the cryostat is mounted on a circular-arc guiding stage. To shutoff the ambient air through the large gap in the hole, the bellows with a slidable flange is installed between the cryostat and the wall paneling. In addition to this, the 1/3 part of the cryostat at the entrance window side is made of stainless steel, whose thermal conductivity is smaller than that of aluminum alloy, to reduce the thermal influx conducted along the cryostat into the refrigerator. When we change the observation mode, the circular-arc guiding stage, the slidable bellows flange, and the tilt and focus stage of the detector are moved all together.

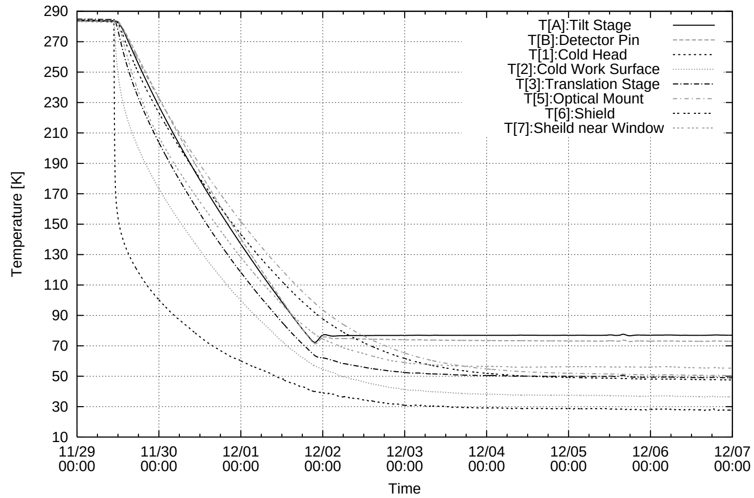

Figure 10. Internal temperature of the camera cryostat during cooling.

The optical bench frame in the refrigerator consists of general aluminum frames, which contract as it cools down (Fig. 7). To cancel these contraction as well as to adjust the focus on the mask mirror from outside of the refrigerator, the mask mirror holder is mounted on a thin linear stage powered by a general pulse motor actuator, and the fiber slit is attached to the 6-axis adjustable stage with Picomotor$^{\mathrm{TM}}$ actuators manufactured by New Focus Inc.[¶], whose rotation of the screws is monitored by rotary potentiometers individually (Fig. 8). The Picomotor$^{\mathrm{TM}}$ actuators are also used in the mosaic grating holder to adjust the direction of the four gratings under refrigerated condition (Fig. 9). The VPH grating holder is mounted on the linear transfer stage controlled by a general pulse motor and a ball spline. We replaced the grease of all the actuators to the low-temperature grease, which enable them to move below $-50°$C.

4. TEST RESULTS

We developed the IRS1 in Kyoto University until June 2005, and then it was shipped to the Subaru Telescope. The reassembling work and the preliminary optical alignment of the IRS1 on the new floor of the Subaru dome was finished in December 2005. After the readout test of the engineering array, the HAWAII2 science array was installed in the camera cryostat. It was cooled down in four days with a typical cooling speed of 4K/hour (Fig. 10).

On the other hand, the cooling test of the refrigerator at full capacity was delayed by a few months due to a replacement of the air-cooled compressor (which we used in Kyoto) by the water-cooled one. Fig. 11 shows the typical cooling curve of the refrigerator tested in Kyoto University. In this case, the inner temperature was almost constant at moderate temperature of $\sim -35°$C, while the wall temperature changes within a controlled temperature range. Although the operation parameter of the refrigerator with the new compressor at the summit has not been fixed yet, we achieved the lowest inner temperature below $-50°$C recently.

We tried to make a fine adjustment using the images on the detector under unstable condition of the refrigerator. To elicit the best performance of the spectrometer, we have to take care of a few extra points as well as the usual optical alignment of an instrument.

First, readjustment of the mosaic grating is required after the inner optics are cooled down because of a small distortion of the inver grating holder as a result of the temperature changes. Fig. 12 shows the image of the infrared laser before and after adjustment of the mosaic grating. The wavelength of the infrared laser is

[¶]http://www.newfocus.com

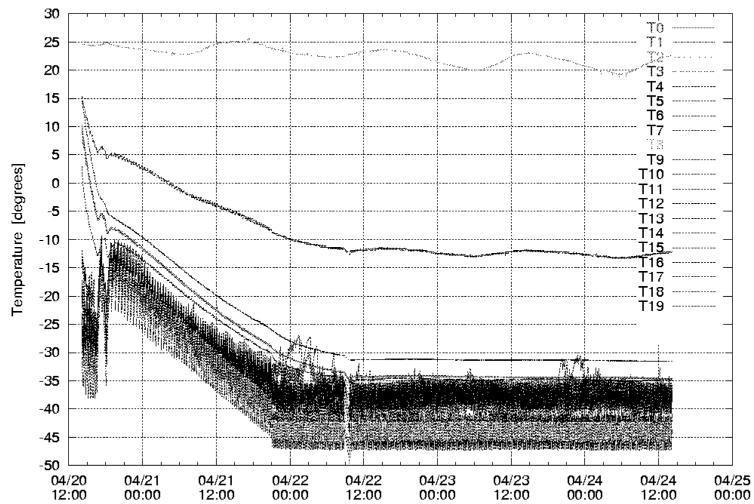

Figure 11. Internal temperature of the refrigerator during cooling. The highest and second-highest curve indicate the outside temperature and the discharge air temperature respectively.

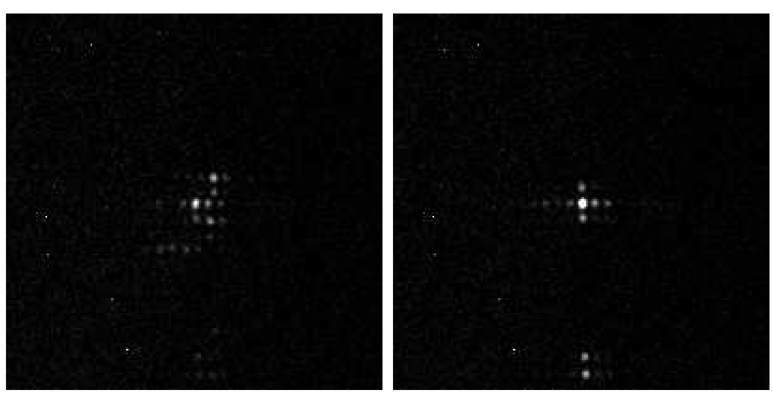

Figure 12. Laser spot image before and after grating adjustment. Many sub-peak features of the laser and the leakage of the light into the nearest fibers blur the real peak.

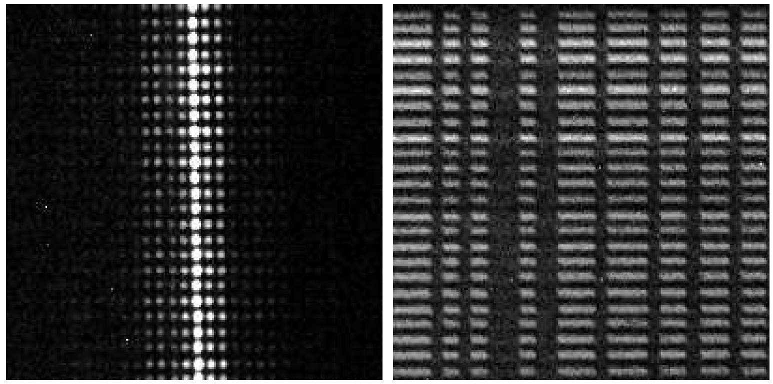

Figure 13. Infrared laser spectra (left) and flashlight continuum spectra (right). Vertical black lines are the image of the airglow mask.

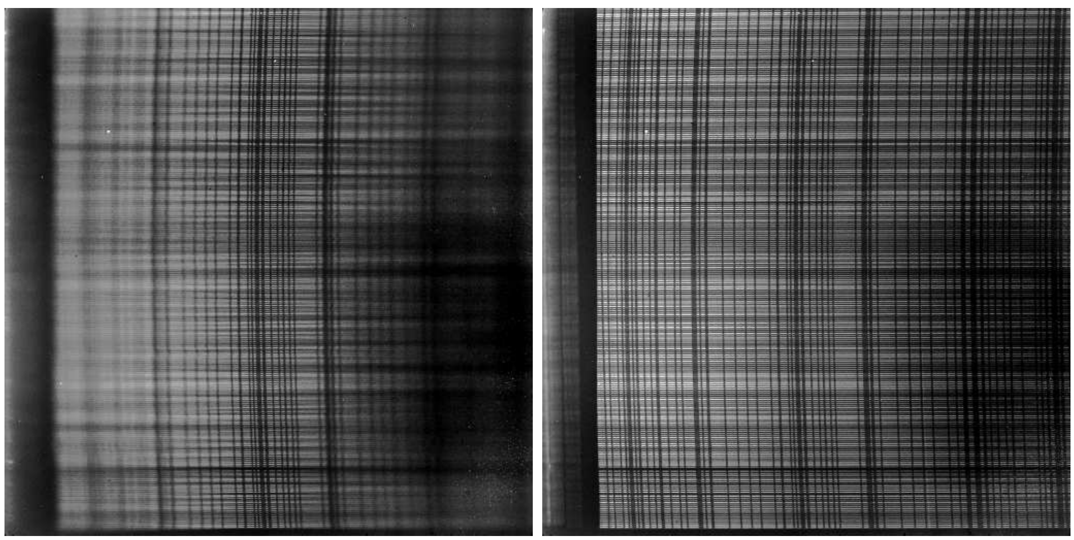

Figure 14. Flashlight continuum image before and after adjustment of the detector tilt stage.

1.3μm with many sub-peak at both sides of the peak wavelength (Fig. 13), which blurs the center of the spot corresponding to each grating together with the leaked light into the nearest fibers. The spot diameter of the brightest image of the fiber after grating adjustment is $\sim$4pixels, consistent with the expected sum of the real image size of 3.5pixels and the optical aberration of 2pixels.

Second, both the primary focus (on the mask mirror) and the secondary focus (on the detector) must be adjusted simultaneously. We can check these focuses by flashlight continuum spectra on the detector (Fig. 13), in which the primary and the secondary focus correspond to the sharpness of the mask edge and the width of the spectrum respectively. The focal position of the mask mirror and the detector are fixed to make the above images sharpest.

Finally, the focal position and the tilt angle of the detector are determined in each observation mode (Fig. 14). These values are registered to move the detector automatically in conjunction with the mode selection.

Although the adjustment of IRS1 at the lowest temperature has not been completed yet, we confirmed the total optical performance of IRS1 is just as we expected. There are still many items should be improved, especially relevant to the airglow mask, ghost images, and the infrared stray light. We will examine them carefully and deal properly with possible defects to approach the completion of the spectrograph.

ACKNOWLEDGMENTS

This work is supported by a Grant-in-Aid for Scientific Research (B), Japan (No. 17403003).

REFERENCES

1. T. Maihara, et al., "Fiber multi-object spectrograph (FMOS) for the Subaru Telescope," in *Optical and IR Telescope Instrumentation and Detectors*, M. Iye, and A. F. Moorwood, ed., *Proc. SPIE* **4008**, pp. 1111–1119, 2000.
2. M. Kimura, et al., "Fibre-Multi-Object Spectrograph (FMOS) for Subaru Telescope," in *Instrument Design and Performance for Optical/Infrared Ground-based Telescopes*, M. Iye, and A. F. Moorwood, ed., *Proc. SPIE* **4841**, pp. 974–984, 2003.
3. S. Eto, et al., "The fiber multi-object spectrograph (FMOS) for the Subaru Telescope III," in *Ground-based Instrumentation for Astronomy*, A. F. Moorwood, and M. Iye, ed., *Proc. SPIE* **5492**, pp. 1314–1318, 2004.
4. P. R. Gillingham, S. Miziarski, M. Akiyama, and V. Klocke, "Echidna: a multifiber positioner for the Subaru prime focus," in *Optical and IR Telescope Instrumentation and Detectors*, M. Iye, and A. F. Moorwood, ed., *Proc. SPIE* **4008**, pp. 1395–1403,, 2000.
5. A. M. Moore, P. R. Gillingham, J. S. Griesbach, and M. Akiyama, "Spine development for the Echidna fiber positioner," in *Instrument Design and Performance for Optical/Infrared Ground-based Telescopes*, M. Iye, and A. F. Moorwood, ed., *Proc. SPIE* **4841**, pp. 1429–1439, 2003.
6. P. Gillingham, D. Correll, J. Dawson, A. M. Moore, R. Muller, S. Smedley, and G. A. Smith, "Echidna: the engineering challenges," in *Ground-based Instrumentation for Astronomy*, A. F. Moorwood, and M. Iye, ed., *Proc. SPIE* **5492**, pp. 1228–1242, 2004.
7. G. J. Murray, G. N. Dodsworth, R. Content, N. Tamura, D. J. Robertson, D. Gedge, and B. Brooks, "An ultraprecision fiber connector for FMOS," in *Ground-based Instrumentation for Astronomy*, A. F. Moorwood, and M. Iye, ed., *Proc. SPIE* **5492**, pp. 1383–1394, 2004.
8. P. R. Gillingham, et al., "The Fiber Multi-object Spectrograph (FMOS) Project: the Anglo-Australian Observatory role," in *Instrument Design and Performance for Optical/Infrared Ground-based Telescopes*, M. Iye, and A. F. Moorwood, ed., *Proc. SPIE* **4841**, pp. 985–996, 2003.
9. I. J. Lewis, et al., "Developments on the UK FMOS project for the Subaru telescope," in *Instrument Design and Performance for Optical/Infrared Ground-based Telescopes*, M. Iye, and A. F. Moorwood, ed., *Proc. SPIE* **4841**, pp. 1108–1114, 2003.
10. I. A. Tosh, et al., "The current status of the UK-FMOS spectrograph," in *Ground-based Instrumentation for Astronomy*, A. F. Moorwood, and M. Iye, ed., *Proc. SPIE* **5492**, pp. 1362–1370, 2004.
11. F. Iwamuro, K. Motohara, T. Maihara, R. Hata, and T. Harashima, "OHS: OH-Airglow Suppressor for the Subaru Telescope," *Publications of the Astronomical Society of Japan* **53**, pp. 355–360, 2001.
12. K. W. Hodapp, et al., "The HAWAII-2 20482048 HgCdTe Detector Arrays," in *Scientific Detectors for Astronomy, The Beginning of a New Era*, P. Amico, J. W. Beletic, J. E. Beletic, pp. 501–509, 2004.